Preprints (www.preprints.org) | NOT PEER-REVIEWED | Posted: 23 December 2020 doi:10.20944/preprints202012.0573.v1

Article

An experimental study of the acetic acid steam reforming over Co-based catalysts

Marta Cortese[1*], Concetta Ruocco[1], Vincenzo Palma[1], P.J. Megía[2], A. Carrero[2] and J.A. Calles[2]

[1] *University of Salerno, Department of Industrial Engineering, Via Giovanni Paolo II 132, 84084 Fisciano (SA), Italy*
[2] *Chemical and Environmental Engineering Group, ESCET, Rey Juan Carlos University, 28933 Móstoles, Spain*
* Correspondence: Marta Cortese, e-mail: mcortese@unisa.it

Abstract: This work focuses on the support effect on the performances of Co-based catalysts for the acetic acid steam reforming. SBA-15, a well ordered hexagonal mesoporous silica structure, and CeO_2 have been selected as the supports, with the impact of chromium addition also being investigated. Better acetic acid steam reforming performances have been recorded for CeO_2 compared to SBA-15 supported catalysts and, in particular, the 7Co/CeO_2 catalyst showed the highest values of acetic acid conversions with enhanced H_2 yields below 480°C, in comparison to the other investigated catalytic formulations. In addition, more pronounced coke depositions and acetone concentrations have been obtained with CeO_2 supported catalysts, due to the tendency of ceria to catalyse the ketonization reaction. Chromium addition to Co/SBA-15 catalysts led to an enhancement in the activity towards acetic acid steam reforming, while on CeO_2 supported catalysts no improvement in the catalysts activity was observed; however, on both SBA-15 and CeO_2 supported catalysts, Cr addition reduced the amount of coke deposited on the catalysts surface.

Keywords: Acetic acid, reforming, hydrogen, cobalt, ceria.

1. Introduction

The increasing levels of CO_2 in the atmosphere, along with the emission of other harmful pollutants (NO_x and SO_2) has led to serious environmental concerns, with experts searching for low-environmental impact sources to solve the current energy crisis. Renewable resources are extremely promising, while the use of biomass as feedstock is encouraged due to its sustainability, wide availability and abundance [1]. Consequently, the use of biomass-derivate compounds (including acetic acid) as a hydrogen source has the potential to reduce the current dependence on fossil fuels [2,3]. Hydrogen is regarded as one of the energetic vectors of the future and its production via reforming of bio-fuels has been widely studied in current literature [4,5]. In 2019, the demand for pure hydrogen was estimated as 70 million tons. The majority of produced hydrogen comes from the conversion of fossil fuels, while only less than 1% hydrogen derives from renewable sources [6]. Among the available feedstocks for hydrogen generation, acetic acid is a promising alternative, with a growing market production expected to reach 18 million tons by 2020 [7].

Acetic acid is mainly produced via methanol carbonylation (~75%) [8]; however, the synthetic route creates severe environmental concerns, due to the release of dangerous by-products and the use of petroleum as feedstock; in addition, this process uses very expensive catalysts. Conversely, extensive research has studied a hydrothermal process [9], which exploits its well-known properties at both high-temperatures and pressures [10]. Other eco-friendly and clean technologies for acetic acid production, including membrane-based processes, are under presently investigation [7].

© 2020 by the author(s). Distributed under a Creative Commons CC BY license.

Preprints (www.preprints.org) | NOT PEER-REVIEWED | Posted: 23 December 2020 doi:10.20944/preprints202012.0573.v1

The conversion of bio-oil obtained via the fast pyrolysis of biomass and its subsequent catalytic steam reforming has been regarded as a feasible and economical route for hydrogen production [11]. Acetic acid is the main component of bio-oil (up to 33%) and its reforming as a bio-oil representative compound has been widely investigated [12]. Bio-based acetic acid steam reforming processes (AcOH-SR) are a potential approach for hydrogen production, which can be directly used in oxide fuel cells or further treated to generate electricity in proton exchange membrane fuel cells [13]. Acetic acid, compared to other biomass-based hydrogen carriers such as ethanol and methanol, is non-flammable and much safer to store and transport [14]. Moreover, the net energy balance for bio-oil production from biomass via integrated fast-pyrolysis is considerably higher than that reported for bioethanol generation (7.01 vs 1.07) [15].

According to the stoichiometry of the acetic acid steam reforming reaction (Eq. 1), one mole of acetic acid can produce four moles of hydrogen, as a result of the thermal decomposition reaction (Eq. 3) and the water gas shift reaction (Eq. 2). However, the theoretical hydrogen yield is commonly vitiated by undesirable products formation, mainly carbon monoxide, methane and acetone. Methane is mainly formed via decarboxylation (Eq. 4) and acetic acid can also be ketonized to acetone (Eq. 5) [16]. C_3H_6O formation is considered one of the principal causes of coke and high condensation products deposition on the catalyst surface, that leads to catalysts deactivation [17,18]. Moreover, a Boudouard reaction (Eq. 6) and methane decomposition (Eq. 7), are also responsible for coke formation and reduced hydrogen selectivities, contributing to the consequent catalysts deactivation [19,20].

AcOH Steam reforming	$CH_3COOH + 2H_2O \leftrightarrows 4H_2 + 2CO_2$	*ΔH= 131.4 kJ/mol*	Eq. 1
Water gas shift	$CO + H_2O \leftrightarrows CO_2 + H_2$	*ΔH= -41.1 kJ/mol*	Eq. 2
Thermal decomposition	$CH_3COOH \leftrightarrows 2H_2 + 2CO$	*ΔH= 213.7 kJ/mol*	Eq. 3
Decarboxylation	$CH_3COOH \leftrightarrows CH_4 + CO_2$	*ΔH= -33.5 kJ/mol*	Eq. 4
Ketonization	$2CH_3COOH \leftrightarrows C_3H_6O + H_2O + CO_2$	*ΔH= 16.7 kJ/mol*	Eq. 5
Boudouard reaction	$2CO \leftrightarrows C + CO_2$	*ΔH= -172.4 kJ/mol*	Eq. 6
Methane decomposition	$CH_4 \leftrightarrows C + 2H_2$	*ΔH= 74.8 kJ/mol*	Eq. 7

The design of a proper catalytic formulation is a critical challenge to maximize hydrogen production and limit activity losses [21]. Several active species have been investigated [22–24], showing that hydrogen selectivity decreased in the order Co>Ni>Rh>Pt [25]. According to numerous studies [25,26], cobalt has a reasonable activity for acetic acid reforming at low temperatures, due to its ability to break down both C-C and C-H bonds, along with its competitive price. Moreover, Co displayed very high activity towards water-gas shift reactions at 550°C. The combination of cobalt with a second metal as a promoter (i.e. nickel or potassium) has shown to improve the coking resistance of the final catalyst, inhibiting, at the same time, the methanation reaction [27,28]. Regarding the choice of the oxide support, alumina is traditionally used for the reforming

Preprints (www.preprints.org) | NOT PEER-REVIEWED | Posted: 23 December 2020 doi:10.20944/preprints202012.0573.v1

process, due to its high surface area and mechanical stability. However, the surface acidity promotes acetone and coke precursors formation. Thus, the performance of different supports, capable of enhancing hydrogen yield and deactivation resistance, has been investigated [29]. SBA-15, instead of common amorphous silica, was reported to be a very useful support, capable of preventing Co particles aggregation and metal sintering [30]. SBA-15, a well ordered hexagonal mesoporous (4-12 nm) silica structure presents several attractive characteristics as a catalytic support, such as high specific surface area (600-1000 $m^2 g^{-1}$), ease of synthesis, high thermal and mechanical stability [31–33]. Garcia et al. [34] reported the beneficial effect of Cr addition to Co-based catalysts, as a promoter towards hydrogenation–dehydrogenation reactions (i.e. coke precursors hydrogenation). Chromium was also shown to be a textural promoter, reducing the crystallite dimensions and limiting the sintering of the active species [35]. Our previous work [36] highlighted the good performance of a Co-Cr/SBA-15 catalyst in terms of high activity, hydrogen yield and low coke deposition. In addition to SBA-15, other supports, including CeO_2, Al_2O_3 and CeO_2-ZrO_2, have shown promising results for hydrogen production via steam reforming [37,38]. The selection of rare earth oxides allows to exploit the oxygen storage and release capacity of these supports, which are beneficial to preventing and/or removing carbon deposits [39–41]. The reversible redox cycle between Ce^{4+} and Ce^{3+} ions generates oxygen vacancies, thus taking or releasing oxygen on the basis of surface requirements and assuring an easy oxidation of carbonaceous species. This property is called as oxygen storage capacity (OSC). An enhancement in coke gasification by steam was reported, along with an improved reforming activity ascribable to the mobile oxygen in the ceria lattice [21]. Thus, ceria not only acts as the support for the active metals but also as an oxygen reservoir; moreover, the choice of ceria with a high-surface area can reduce the impact of sintering which, together with the boosted contribution of coke gasification, is expected to improve the catalyst activity and stability [42,43].Moreover, to the best of our knowledge, Co-Cr/CeO_2 catalysts have yet to be investigated for acetic acid steam reforming. In this study, ceria was therefore chosen as the support to disperse cobalt and chromium.

In this work, a series of Co and Co-Cr catalysts supported on SBA-15 or CeO_2 was prepared, characterized by means of TPR (Temperature Programmed Reduction), XRD (X-ray Diffraction method), ICP-AES (Inductively Coupled Plasma Atomic Emission Spectrophotometry), TEM (Transmission Electron Microscope) and SSA (Specific Surface Area) analysis, and subsequently their catalytic activities investigated between 400 and 600°C, in order to study the influence of the adopted support and the chromium effect on the catalysts performances in terms of acetic acid conversion and hydrogen yield.

2. Materials and Methods

2.1. Preparation and characterization of the catalysts

Co and Co-Cr catalysts, supported over mesostructured SBA-15 material, were prepared through the incipient wetness impregnation and co-precipitation method using $Co(NO_3)_2{\cdot}6H_2O$ and $Cr(NO_3)_3{\cdot}9H_2O$ as precursor salts, as described elsewhere [30]. The SBA-15, used as the support, was synthetized according the hydrothermal method described for the first time by Zhao [31]. On the other hand, mono and bi-metallic CeO_2 supported catalysts were prepared through a wet impregnation and co-precipitation method using $Co(NO_3)_2{\cdot}6H_2O$ and $Cr(NO_3)_3{\cdot}9H_2O$ as precursor salts. Commercial CeO_2 (ACTALYS® HSA 5 purchased by Solvay) was adopted as a support; it was first calcined at 600°C for 3h and subsequently impregnated in a solution of the Co and Cr salts precursors at 120°C until complete water evaporation. Afterwards, the obtained powder catalysts were dried and calcined at 600°C for 3h.

Preprints (www.preprints.org) | NOT PEER-REVIEWED | Posted: 23 December 2020 doi:10.20944/preprints202012.0573.v1

Table 1 presents a list of the catalytic formulations prepared in this work.

Preprints (www.preprints.org) | NOT PEER-REVIEWED | Posted: 23 December 2020 doi:10.20944/preprints202012.0573.v1

Table 1. Summary of the synthesized catalysts.

Sample	*Support*	*Co content, wt.%*	*Cr content, wt.%*
7Co/SBA-15	*SBA-15*	*7*	-
2Cr7Co/SBA-15	*SBA-15*	*7*	*2*
7Co/CeO_2	*CeO_2*	*7*	-
2Cr7Co/CeO_2	*CeO_2*	*7*	*2*
3Cr12Co/CeO_2	*CeO_2*	*12*	*3*

The prepared catalysts were characterized by means of TPR analysis, SSA determination, XRD and ICP-AES.

Samples reducibility was evaluated through TPR analysis, carried out in-situ under a reducing stream (5% H_2/Ar) and heating up the reactor from room temperature to 600°C with a 5°C/min heating rate.

TEM micrographs were obtained through a Philips TECNAI 20 microscope (200 kV) with a resolution of 0.28 nm.

The SSA analysis was realized in a Costech International Sorptometer 1040 Kelvin. The samples were degassed at 105°C for 30 min and then, the SSA evaluation performed by N_2 dynamic adsorption at -196°C; then, the SSA determination was obtained through the B.E.T. equation.

The Co and Cr contents in the prepared catalysts were determined using ICP-AES in a Varian VISTA-PRO AX CCD-Simultaneous ICP-AES spectrophotometer. The samples were previously treated by acidic digestion using H_2SO_4 and HF.

All the X-ray diffraction measurements were collected at room temperature by means of a Philips X'pert PRO diffractometer using Cu Kα radiation and, subsequently, the Scherrer equation was used to calculate the mean crystallite sizes.

2.2. Experimental activity

All the experimental tests were conducted using a tubular fixed-bed reactor (AISI 316L stainless steel 37 cm, o.d. 13 mm, i.d. 9 mm), in which the catalyst was fixed between quartz wools; the reactor was placed vertically in a heated furnace and the gas temperature was measured in correspondence to the end section of the catalytic bed by means of a K-type thermocouple.

The H_2O/AcOH liquid mixture, stored in a tank under nitrogen pressure and fed by a mass flow controller for liquids, was firstly mixed with argon, and then sent to a stainless-steel boiler at 260°C, in order to reach a complete vaporization and good mixing of the total reactor inlet flow rate. Furthermore, the boiler outlet mixture, by means of two 4-ways valves, could be alternatively sent to either the reactor or the purge, reaction or bypass configurations, through ¼" stainless steel pipes, heated at 160°C, to avoid any possible condensations. In the bypass configuration, nitrogen could be used as the inert gas in the operations of heating up or cooling down.

The reactor outlet products stream was continuously analysed by means of a Hiden Analytical mass spectrometer, observing 2, 16, 18, 28, 40, 43, 44 and 58 fragments in order to evaluate the concentration of H_2, CH_4, H_2O, CO, Ar, AcOH, CO_2 and C_3H_6O, respectively. A scheme of the experimental set up in the tests is presented in Figure 1:

Preprints (www.preprints.org) | NOT PEER-REVIEWED | Posted: 23 December 2020 doi:10.20944/preprints202012.0573.v1

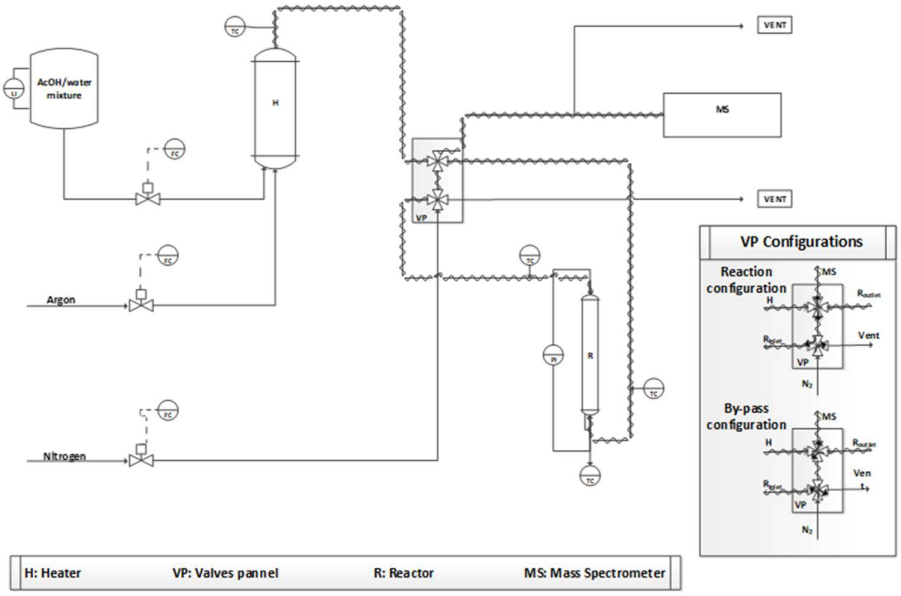

Figure 1. Scheme of the experimental set up.

All the prepared catalytic formulations were tested under the same experimental conditions, with a WHSV (Weight Hourly Space Velocity) of 30 h^{-1}, defined as the ratio between the total mass flow rate fed to the reactor and the amount of catalyst loaded into the reactor. The feeding mixture was composed of volumetric percentages of 10%AcOH, 40%H_2O and 50%Ar, characterized by a H_2O/AcOH molar ratio equal to 4. Furthermore, as the different tested catalysts presented various density values, in order to have comparable fluid dynamic conditions in all the tests, 1g of powder catalyst (180-355 μm) was diluted with different amounts of 500÷710 μm quartz flakes to keep constant a total bed volume of 2,5 cm^3.

Prior to the evaluation of the catalytic performances, the carbon, hydrogen and oxygen balances closure were checked to ensure the validity of the experimental results, with an error lower than 5% being considered acceptable.

Furthermore, the catalytic performances were evaluated in terms of AcOH conversion (X_{AcOH}), H_2 yield (Y_{H2}) and C_3H_6O yield (Y_{C3H6O}) with the below formulas, where *n* represents the number of moles.

$$X_{AcOH} = \frac{n_{AcOH,in} - n_{AcOH,out}}{n_{AcOH,in}} \cdot 100\% \qquad \text{Eq. 8}$$

$$Y_{H_2} = \frac{n_{H_2}}{4 \cdot n_{AcOH,in}} \qquad \text{Eq.9}$$

$$Y_{C_3H_6O} = \frac{2 \cdot n_{C_3H_6O}}{n_{AcOH,in}} \qquad \text{Eq. 10}$$

The experimental procedure was as follows: prior to any catalytic test, the samples were reduced as reported in Section 2.1. Subsequently, the catalysts activity was evaluated in the temperature range of 600°C - 400°C in a descending order, with a cooling rate of 2°C/min.

After each run, the carbon deposition was evaluated in terms of Carbon Formation Rate (CFR), defined as follows (Eq. 11):

$$CFR = \frac{mg_{coke}}{g_{Carbon,fed} \cdot h \cdot g_{catalyst}} \qquad \text{Eq. 11}$$

Preprints (www.preprints.org) | NOT PEER-REVIEWED | Posted: 23 December 2020 doi:10.20944/preprints202012.0573.v1

in which: mg_{coke} [g] indicates the total amount of coke deposited during the test, $g_{Carbon,fed}$ [g] represents the whole quantity of carbon fed during the reaction experiments, h [h] the time elapsed and $g_{catalyst}$ [g] the weight of catalyst loaded in the reactor.

The carbon formation rate expression has been already reported for reforming reactions [44]. The amount of carbon deposits on the catalysts surface was estimated by exposing the spent catalyst to air and heating up to 600°C (2°C/min) and evaluating the consequent difference in weight.

3. Results and Discussion

3.1. Catalysts characterization

The SSA analysis, carried out on the supports and the examined catalytic formulations, are given in Table 2 in which it is possible to note that the SBA-15 samples present higher SSA compared to the CeO_2 based catalysts. Moreover, the chromium addition to $7Co/CeO_2$ induces a drastic decrease in the specific surface area of the catalysts compared to the SBA-15 based catalysts. The Cr addition to $7CoCeO_2$ lowers the SSA of the 30%, while 2Cr7Co/SBA-15 presents a decrease in the SSA value of only 11%, thus suggesting that the chromium addition on the ceria catalysts may cause a pore filling that lowers the SSA of the catalysts.

Table 2. Results of the specific surface area determination for the analyzed catalysts.

Sample	*SSA, $m^2 g^{-1}$*
SBA-15	*465*
7Co/SBA-15	*406*
2Cr7Co/SBA-15	*362*
CeO_2	*105*
$7Co/CeO_2$	*88*
$2Cr7Co/CeO_2$	*62*
$3Cr12Co/CeO_2$	*45*

Preprints (www.preprints.org) | NOT PEER-REVIEWED | Posted: 23 December 2020 doi:10.20944/preprints202012.0573.v1

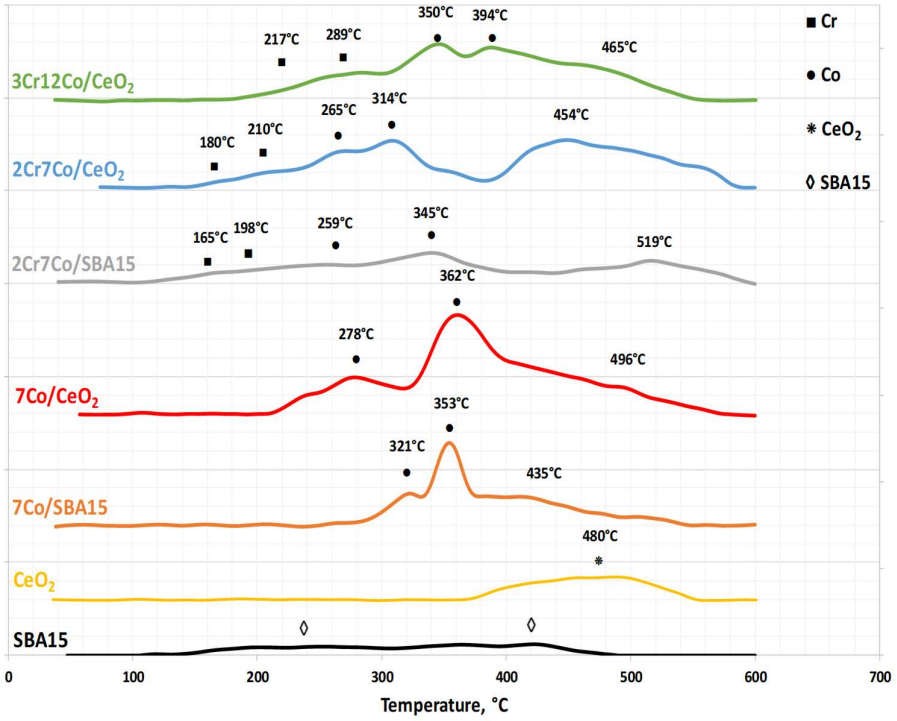

Figure 2. TPR profiles of the tested catalytic formulations and supports.

Regarding the H_2 reduction tendency, as reported in current literature, Co supported catalysts are characterized by two main reduction peaks in the range of 300-400°C, that correspond to the reductions of Co_3O_4 to CoO and CoO to Co^0, respectively, and an additional broad peak, detected at higher temperatures, resulting from the interactions with the support [45], while crystalline chromia presents a main peak at 250°C with a shoulder at 180°C and a weak one at about 360°C [46].

Figure 2 shows the H_2 consumption trends as function of temperature; not appreciable H_2 consumption was detected for SBA-15, while CeO_2 exhibits a characteristic peak around 480°C [47]. Moreover, the presence of the two Co reduction main peaks was encountered for all the analysed samples, whilst the maxima temperature and the intensity of the third peak was strongly affected by the support effect. Comparing 7Co/SBA-15 and 7Co/CeO_2, the latter showed a more intense peak at higher temperatures, ascribable to the reduction of Co oxides along with the reduction of the surface shell of Ceria, promoted by the presence of cobalt metal, as reported in current literature [48,49], while the peak showed by 7Co/SBA-15 at higher temperatures may depend on the strong interaction between cobalt oxide particles and the mesoporous support [50,51]. Chromium low temperature reduction peaks have been detected for all the Cr-containing samples, whereas the higher temperature peak resulted overlapped with the cobalt reduction. The Cr addition results in a leftward shift of the cobalt peaks: both 2Cr7Co/SBA-15 and 2Cr7Co/CeO_2 present lower Co reduction temperatures, indicating lower interaction with the support and/or better active species dispersion [36]; furthermore, the analysis on the 3Cr12Co/CeO_2 highlights that an increase in the Cr content causes a shift of the Co peaks to higher temperatures, thus suggesting a mutual interaction between cobalt and chromium species, as described by Chen et al. [52].

Preprints (www.preprints.org) | NOT PEER-REVIEWED | Posted: 23 December 2020 doi:10.20944/preprints202012.0573.v1

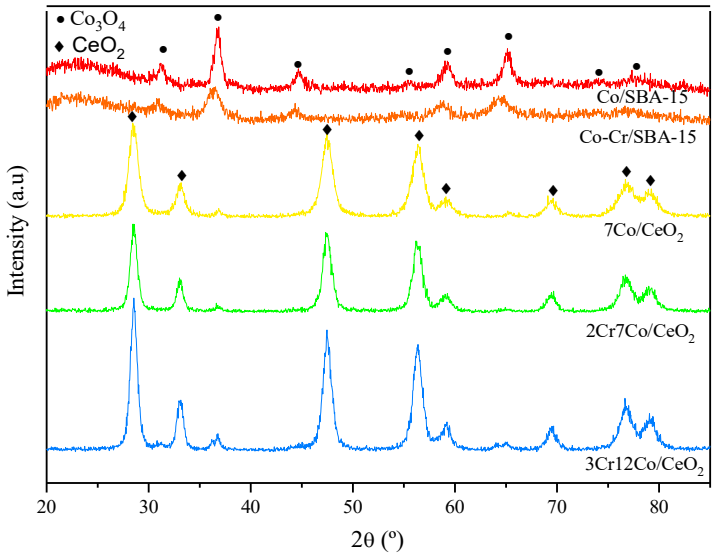

Figure 3. XRD spectra of the investigated catalysts.

Figure 3 shows the XRD patterns of the calcined samples. Peaks attributed to cubic Co_3O_4 appear in Co-based catalysts supported over SBA-15 at 2θ = 31.4º, 37.1º, 45º, 56º, 59.7º, 65.6º, 74.5º and 77.8º (JCPDS 01-071-4921) corresponding to the (220), (311), (400), (422), (511), (440), (620) and (533) reflection planes, respectively. Regarding the Co-based catalyst supported over CeO_2, only peaks with a refection at 2θ = 37.1º, 44,9º and 65.6º are distinguished, since the diffraction spectra indicated the well-defined and high-intensity major peaks of cubic CeO_2 (JCPDS 01-089-8436), which is constituting the support. These peaks showed the refection at 2θ = 28.6º, 33.1º, 47.5º, 56.4º, 59.1º, 69.4º, 76.7º and 79.1º. Cr-oxides were not detected in 2Cr7Co/SBA-15, 2Cr7Co/CeO_2 and 3Cr 12Co/CeO_2 due to the overlap between the highest diffraction peaks of orthorhombic Cr_2O_3 (JCPDS 00-071-4807) with those of the Co_3O_4 pattern. Furthermore, since the Co content was much higher than the Cr content in all the prepared catalysts, these peaks would have a negligible effect on the XRD patterns, being the Cr species well-dispersed over the support as reported elsewhere [55].

Moreover, from the analysis of the crystallites dimensions performed using the Scherrer equation, it is possible to note in Table 3 that the addition of chromium to both the SBA-15 and CeO_2 supported catalysts, remarkably decreased the Co crystallites sizes, thus probably leading to a higher dispersion of the metal species; these results are expected to assure a better AcOH-SR performance.

Table 3. Metal contents in the samples obtained by ICP analysis and diameters of the Co_3O_4 crystallite calculated using the Scherrer equation, from the (311) diffraction plane of Co_3O_4.

Sample	*Co content, wt.%*	*Cr content, wt.%*	$d_{Co_3O_4}$, *nm*
7Co/SBA-15	*6.9*	-	*10*
2Cr7Co/SBA-15	*6.7*	*1.8*	*6*
7Co/CeO_2	*5.6*	-	*18*
2Cr7Co/CeO_2	*6.4*	*1.9*	*14*
3Cr12Co/CeO_2	*9.5*	*3.0*	*14*

Preprints (www.preprints.org) | NOT PEER-REVIEWED | Posted: 23 December 2020 doi:10.20944/preprints202012.0573.v1

ICP analysis was used to estimate the metals weight percentages in the prepared samples; in Table 3 is possible to observe that, while for the SBA-15 supported catalysts the metal content corresponds to the estimated amounts, the CeO_2 supported samples are characterized by a Co content lower than the predicted values.

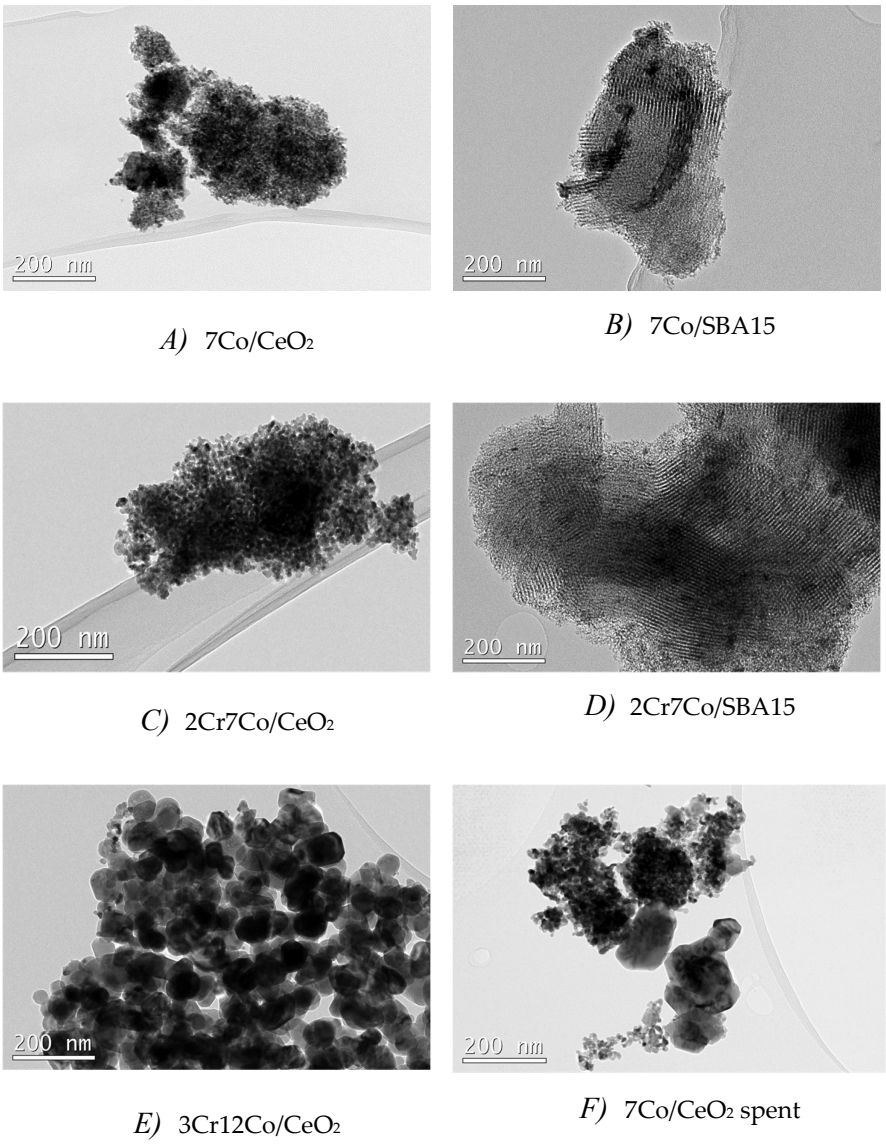

A) 7Co/CeO_2 *B)* 7Co/SBA15

C) 2Cr7Co/CeO_2 *D)* 2Cr7Co/SBA15

E) 3Cr12Co/CeO_2 *F)* 7Co/CeO_2 spent

Figure 4. TEM images of the catalysts

In Figure 4 the TEM images of the tested catalysts are shown. As it is possible to notice, CeO_2 and SBA-15 supported catalysts display different structures; indeed, in the SBA-15 supported catalysts, the well ordered hexagonal mesoporous silica structure is clearly visible from the TEM images (see Figure 4B) and D)), while for the ceria supported samples the structure of the catalysts appears as agglomerates of spherical particles. Moreover, the dispersion of the active species seems to be higher on the catalysts supported on ceria, thus probably leading to higher performances of the catalysts. In addition TEM analysis was also performed on the sample 7Co/CeO_2 spent (after the activity test), and as it is possible to see from Figure 4F), the presence of consistent agglomerate of coke was obtained.

Preprints (www.preprints.org) | NOT PEER-REVIEWED | Posted: 23 December 2020 doi:10.20944/preprints202012.0573.v1

3.2. Activity tests

3.2.1. Homogeneous reaction

In order to quantify the contribution of the reaction in the absence of catalysts, a homogeneous reaction test was performed, with the same conditions adopted for the catalytic experiments (AcOH:H_2O:Ar = 1:4:5), but with only quartz flakes within the reactor. Figure 5 shows that a maximum value of 20% was reached for AcOH conversion, descending, however, to zero at 500°C and giving a low H_2 yield and a considerable C_3H_6O yield. Moreover, analyzing the products distribution presented in Figure 6, it can be appreciated the presence in the product streams of CO and CO_2, while methane was not detected, thus suggesting that thermal decomposition and ketonization reactions were taking place, whilst the exothermic decarboxylation was suppressed. Furthermore, no decrease in the water concentration was detected at the reactor outlet (not reported in the graphs), leading to the conclusion that the water gas shift reaction was not occurring.

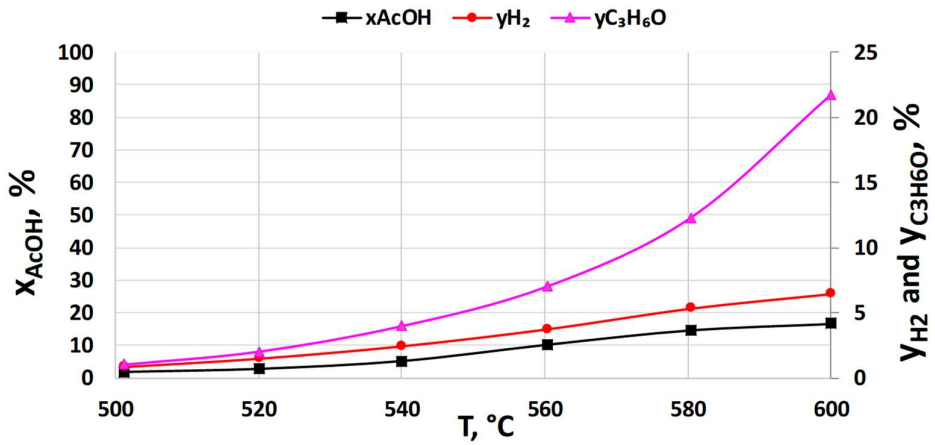

Figure 5. AcOH conversion, H_2 yield, C_3H_6O yield as a function of temperature for the AcOH-SR homogeneous reaction test.

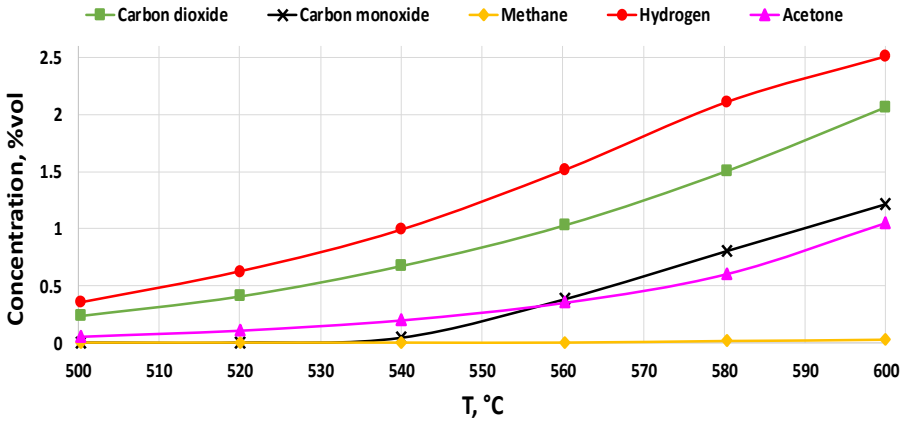

Figure 6. Products distribution as a function of temperature for the AcOH-SR homogeneous reaction test.

3.2.2. Support effect

Carrying out the AcOH-SR with CeO_2 or SBA-15, without the presence of the active phase, led to different results in terms of AcOH conversion, H_2 yield and C_3H_6O yield, as depicted in Figure 7. The obtained data showed higher acetic acid conversions and H_2 yields on ceria (100% AcOH and ~10% H_2 yield at 600°C) compared to SBA-15 (23% AcOH

Preprints (www.preprints.org) | NOT PEER-REVIEWED | Posted: 23 December 2020 doi:10.20944/preprints202012.0573.v1

and ~2% H_2 yield at 600°C); however, the conversion dropped to zero at 500°C, as in the case of the homogeneous reaction. While, on SBA-15, around 530°C the conversion dropped to zero, so the test was stopped before reaching the lowest value of the planned temperature.

In addition, the support choice strongly affected the acetone selectivity of the sample, causing an opposite behavior in terms of acetone formation. While with SBA-15 only a slight concentration of acetone was detected, predominantly at higher temperatures, CeO_2 selection resulted in the promotion of C_3H_6O formation, especially when the temperature decreased; although the ketonization mechanism is still widely debated in current literature, it has been proved the tendency of CeO_2 to convert acetic acid in acetone [56,57]. Moreover, the carbon deposition results, shown in Figure 8 in terms of CFR, show the more pronounced tendency of CeO_2 towards coke formation [17]. Earth metal oxides, compared to silica, are particularly prone to ketones formation, even without the presence of an active metal, due to their acid-base properties [58,59].

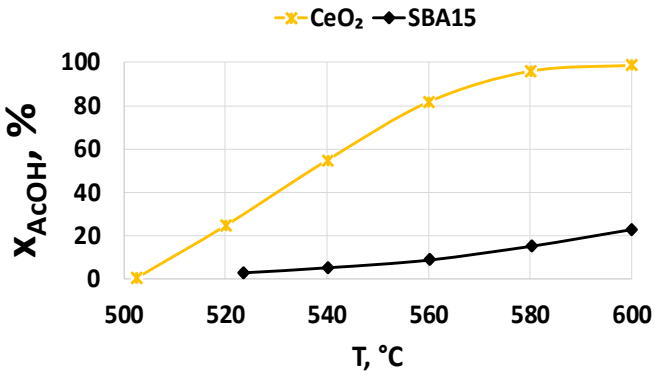

(a)

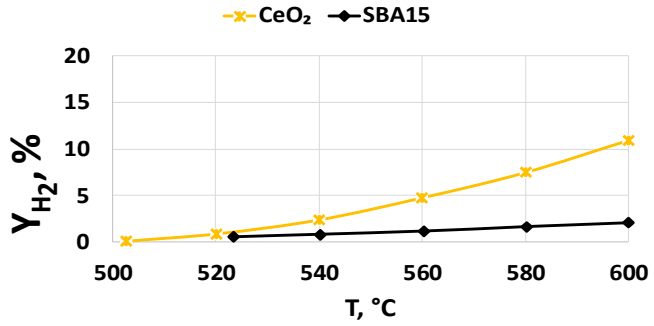

(b)

Preprints (www.preprints.org) | NOT PEER-REVIEWED | Posted: 23 December 2020 doi:10.20944/preprints202012.0573.v1

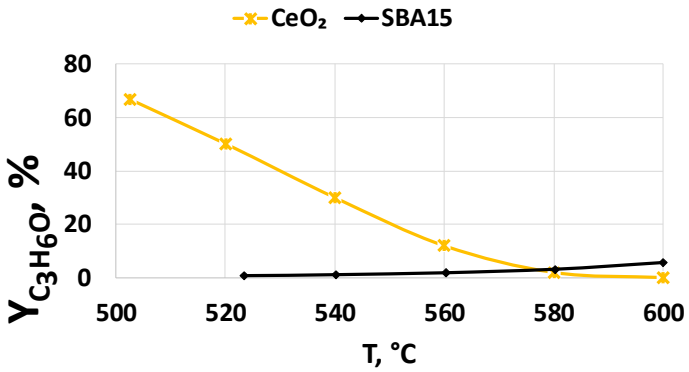

(c)

Figure 7. Trends of X_{AcOH} (a), Y_{H_2} (b) and $Y_{C_3H_6O}$ (c) as a function of temperature in the AcOH-SR over CeO_2 and SBA-15

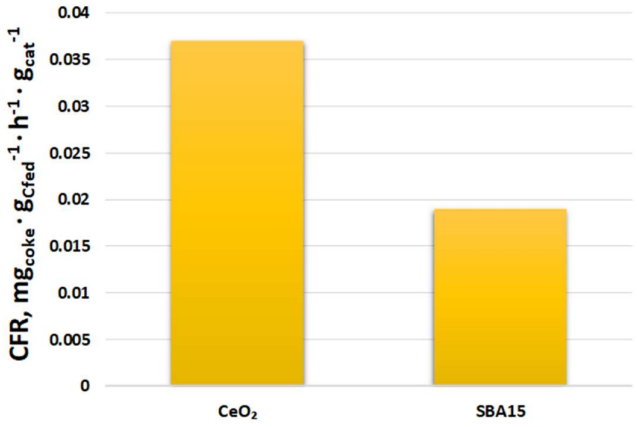

Figure 8. Results of the carbon deposition analysis on the supports.

3.3.3. Catalysts activity tests

In Figure 9, a comparison in terms of X_{AcOH} as a function of reaction temperature shows that, between the tested catalytic formulations, the best performances were achieved for 7Co/CeO_2, that exhibited a conversion higher than 90% from 450°C to 600°C.

Compared to the CeO_2 based catalysts, the SBA-15 supported sample displayed, in general, lower AcOH-SR activity. However, the addition of chromium increased the activity of the SBA-15 catalyst, causing a pronounced enhancement of the acetic acid conversion. An opposite behavior was obtained for the CeO_2 supported catalysts; an increase in the Cr content worsened the catalytic performances of the latter samples in terms of AcOH conversion. This result can be explained by looking at the characterization results commented in Section **Error! Reference source not found.**; the elevated decrease of the specific area observed upon Cr addition to 7Co/CeO_2, probably due to a pore filling effect, led to decreased catalyst performances and lower AcOH-SR activity.

Preprints (www.preprints.org) | NOT PEER-REVIEWED | Posted: 23 December 2020 doi:10.20944/preprints202012.0573.v1

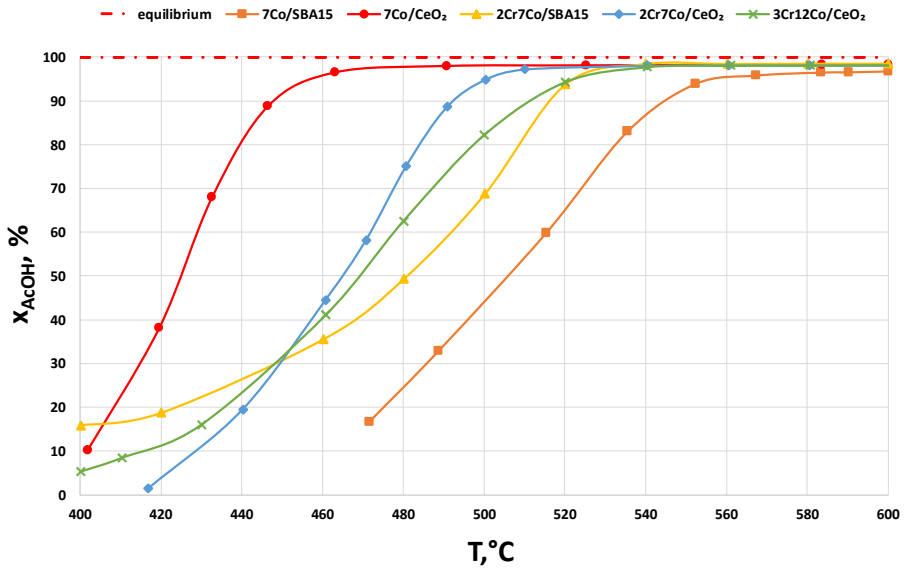

Figure 9. Comparison between the tested catalytic formulations in terms of AcOH conversion as a function of temperature (WHSV=30h^{-1}, AcOH:H_2O:Ar = 1:4:5).

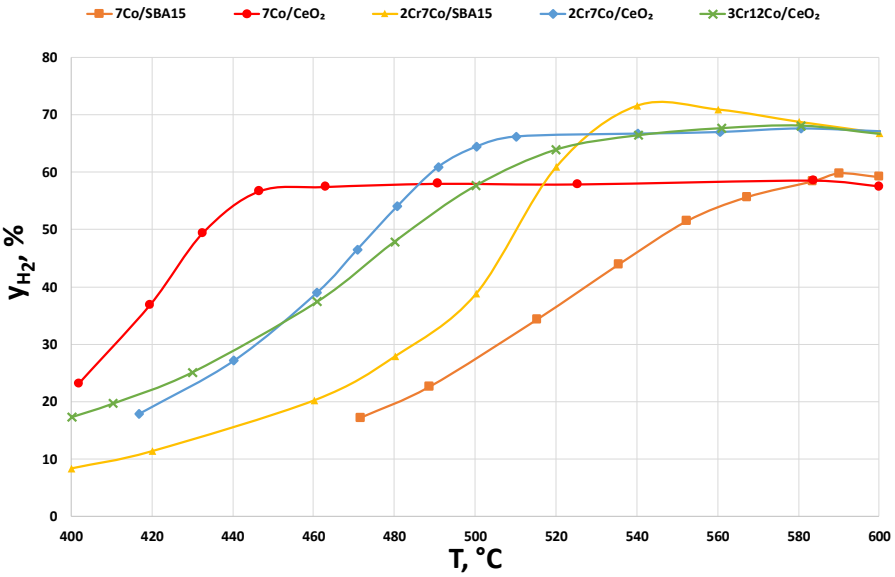

Figure 10. Comparison between the tested catalytic formulations in terms of H_2 yield as a function of temperature

Even though the best performances in terms of AcOH conversions were obtained for the catalyst 7Co/CeO_2, higher H_2 yields were gained, as can be seen in Figure 10, above 500°C, with the addition of chromium; a moderate increase in the H_2 yield was observed for all the Cr- containing samples. This phenomenon, observed for both the CeO_2 and SBA-15 supported catalysts, may be due to the presence of smaller Co particles, obtained after the chromium addition (see section **Error! Reference source not found.**), thus resulting in a better Co dispersion. However, below 480°C, higher H_2 yields are obtained for 7Co/CeO_2 compared with the other catalytic formulations, thus suggesting that the Cr addition has only a slight effect in increasing AcOH-SR performances over the Co/CeO_2 catalysts.

Preprints (www.preprints.org) | NOT PEER-REVIEWED | Posted: 23 December 2020 doi:10.20944/preprints202012.0573.v1

The results presented in Figure 11, together with the X_{AcOH} trends (see Figure 9), confirmed the strict interconnection between the acetone formation and the catalysts loss in activity; since acetone was being detected at the reactor outlet, a rapid decrease of the AcOH conversion was observed.

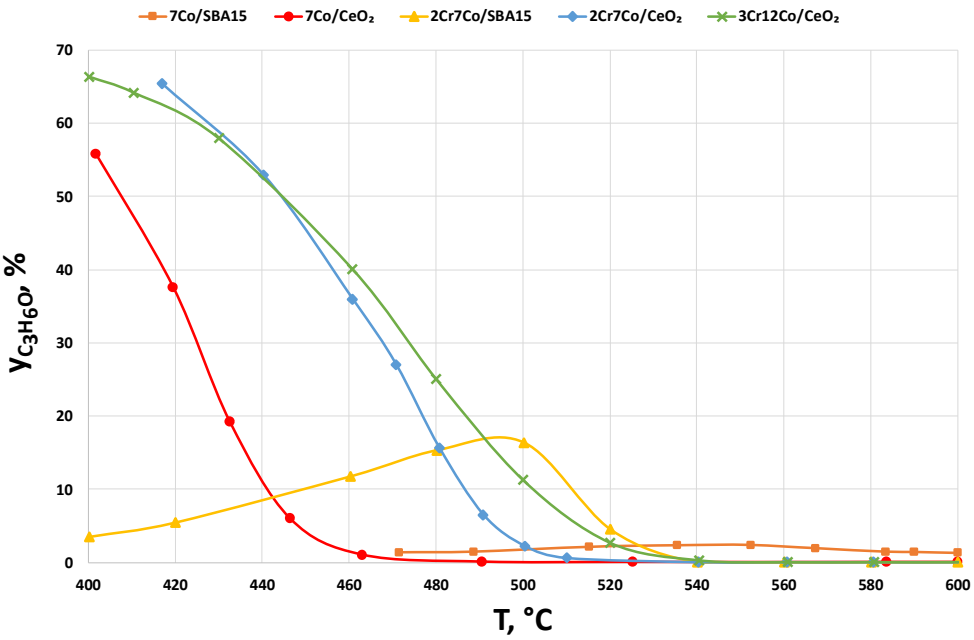

Figure 11. Comparison between the tested catalytic formulations in terms of C_3H_6O yield as a function of temperature

Moreover, coupling the results relating to the C_3H_6O yields with the carbon deposition analysis, depicted in Figure 12, it is possible to better explain the different coke selectivity of mono- and bi-metallic catalysts. 7Co/SBA-15 showed high values of coke deposits, for which a slight C_3H_6O formation was observed already at high temperatures (~600°C), thus suggesting that the low C_3H_6O concentrations, observed at the reactor outlet, were ascribable to acetone decomposition and coke deposits formation; a similar phenomenon has already been reported in current literature on a ZrO_2 supported catalyst [18]. The addition of chromium to 7Co/SBA-15 enhanced the catalyst stability, significantly reducing the amount of coke formed (~0.20 $mg_{coke}/(g_{Cfed} \cdot h \cdot g_{cat})$ for 2Cr7Co/SBA-15 compared to ~0.29 $mg_{coke}/(g_{Cfed} \cdot h \cdot g_{cat})$ for 7Co/SBA-15); although at ~520°C acetone was detected at the reactor outlet and the AcOH conversion dropped to low values, at lower temperatures (~480°C) C_3H_6O yields decreased, leading to a reduced amount of deposited coke for 2Cr7Co/SBA-15 compared to 7Co/SBA-15; this aspect can be seen in Figure 11, in which the peak present in the acetone yield trend clearly suggests that, below 480°C, the acetone concentration is lowered, maybe due to the presence of acetone reforming reactions or due to the inhibition of the ketonization reaction. A similar behaviour was observed for the CeO_2 supported catalysts upon chromium deposition; the interconnection between acetone appearance and the catalysts loss in activity was also encountered on the CeO_2 catalysts.

The 7Co/CeO_2 catalyst exhibited no acetone traces and conversions >90% above 460°C, while for 2Cr7Co/CeO_2 and 3Cr12Co/CeO_2 the conversion dropped, and the acetone formation was already observed at higher temperature values (~500°C). Carbon deposition decreases according to the order: 7Co/CeO_2>2Cr7Co/CeO_2>3Cr12Co/CeO_2, highlighting the advantage obtained with the Cr addition in terms of coke formation: an increase in the chromium content leads to lower carbon depositions. However, contrary to what was observed for the SBA-15 supported catalysts, between the CeO_2 based samples, the catalyst that exhibited the highest value of deposited coke was also characterized by

Preprints (www.preprints.org) | NOT PEER-REVIEWED | Posted: 23 December 2020 doi:10.20944/preprints202012.0573.v1

higher AcOH conversion values (see Figure 9). This result can be ascribed to the improved activity of CeO_2 based catalysts towards both acetic acid reforming and ketonization reaction, as already discussed for the bare supports.

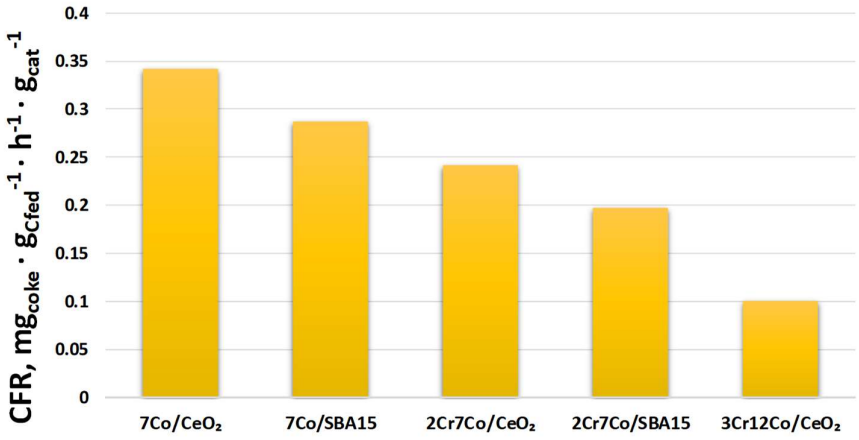

Figure 12. Results of the carbon deposition analysis carried out after each activity test on the spent catalysts.

4. Conclusions

In this work, a series of Co and Co-Cr catalysts supported on SBA-15 or CeO_2 was prepared, characterized by means of TPR, XRD, ICP and SSA analysis, and subsequently tested in the ACOH-SR in order to study the influence of the adopted support ant the chromium addition effect on the catalytic performances.

Carrying out the AcOH-SR on the bare supports (SBA-15 and CeO_2) highlighted their different products selectivities: CeO_2 use, compared to SBA-15, led to obtain higher acetic acid conversions and H_2 yields, but also higher C_3H_6O concentrations and coke deposits, due to the tendency of CeO_2 to catalyse the ketonization reaction.

The activity tests, performed on the different catalytic formulations, showed that the Cr addition to Co-based catalysts had different results depending on the support used. A chromium addition to Co/SBA-15 catalysts led to an enhancement in the AcOH-SR performances, thus resulting in an enhancement of the AcOH conversion, while on CeO_2 supported catalysts, there was no improvement. This behaviour could be explained as follow: the addition of Cr to Co/CeO_2 supported catalysts resulted in reduced Co particles dimensions on the catalysts surface, as in the case of SBA-15 supported catalysts, but the higher SSA decrease, probably due to a pore filling effect. The increase of the chromium content in the catalysts causes a worsening in AcOH conversion and H_2 yields while the only obtained advantages are gained in terms of coke deposition. In order to better exploit the CeO_2 properties, an advantageous opportunity could be the use of more basic promoters, capable of inhibiting ketonization reactions.

Author Contributions: Conceptualization, M.C. and C.R.; methodology, V.P.; software, P.J.M.; validation, P.J.M., A.C. and J.A.C.; formal analysis, C.R.; investigation, M.C.; resources, V.P.; data curation, M.C.; writing—original draft preparation, M.C.; writing—review and editing, V.P.; visualization, C.R..; supervision, V.P.; project administration, V.P.; All authors have read and agreed to the published version of the manuscript.

Funding: This research received no external funding.

Informed Consent Statement: Informed consent was obtained from all subjects involved in the study.

Conflicts of Interest: The authors declare no conflict of interest.

Preprints (www.preprints.org) | NOT PEER-REVIEWED | Posted: 23 December 2020 doi:10.20944/preprints202012.0573.v1

References

[1] Domine, M.E.; Iojoiu, E.E.; Davidian, T.; Guilhaume, N.; Mirodatos, C. Hydrogen production from biomass-derived oil over monolithic Pt- and Rh-based catalysts using steam reforming and sequential cracking processes. *Catal. Today.* **2008** 565–573. https://doi.org/10.1016/j.cattod.2007.12.062.

[2] Assaf, P.G.M.; Nogueira, F.G.E.; Assaf, E.M. Ni and Co catalysts supported on alumina applied to steam reforming of acetic acid: Representative compound for the aqueous phase of bio-oil derived from biomass. *Catal. Today.* **2013** 2–8. https://doi.org/10.1016/j.cattod.2013.02.012.

[3] Adamu, S.; Xiong, Q.; Bakare, I.A.; Hossain, M.M. Ni/Ce-Al_2O_3 for optimum hydrogen production from biomass/tar model compounds: Role of support type and ceria modification on desorption kinetics. *Int. J. Hydrogen Energy.* **2019** 15811–15822. https://doi.org/10.1016/j.ijhydene.2018.12.136.

[4] Bej, B.; Bepari, S.; Pradhan, N.C.; Neogi, S. Production of hydrogen by dry reforming of ethanol over alumina supported nano-NiO/SiO_2 catalyst. *Catal. Today.* **2017** 58–66. https://doi.org/10.1016/j.cattod.2016.12.010.

[5] Spallina, V.; Matturro, G.; Ruocco, C.; Meloni, E.; Palma, V.; Fernandez, E.; Melendez, J.; Pacheco Tanaka, A.D.; Viviente Sole, J.L.; van Sint Annaland, M.; Gallucci, F. Direct route from ethanol to pure hydrogen through autothermal reforming in a membrane reactor: Experimental demonstration, reactor modelling and design. *Energy.* **2018** 666–681. https://doi.org/10.1016/j.energy.2017.11.031.

[6] Safari, F.; Dincer, I.; A review and comparative evaluation of thermochemical water splitting cycles for hydrogen production. *Energy Convers. Manag.* **2020** 112-182. https://doi.org/10.1016/j.enconman.2019.112182.

[7] Pal, P.; Nayak, J. Acetic Acid Production and Purification: Critical Review Towards Process Intensification. *Sep. Purif. Rev.* **2017** 44–61. https://doi.org/10.1080/15422119.2016.1185017.

[8] Vashisht, A.; Thakur, K.; Kauldhar, B.S.; Kumar, V.; Yadav, S.K. Waste valorization: Identification of an ethanol tolerant bacterium Acetobacter pasteurianus SKYAA25 for acetic acid production from apple pomace. *Sci. Total Environ.* **2019** 956–964. https://doi.org/10.1016/j.scitotenv.2019.07.070.

[9] Huo, Z.; Fang, Y.; Yao, G.; Zeng, X.; Ren, D.; Jin, F. Improved two-step hydrothermal process for acetic acid production from carbohydrate biomass. *J. Energy Chem.* **2015** 207–212. https://doi.org/10.1016/S2095-4956(15)60302-3.

[10] Jin, F.; Zhou, Z.; Kishita, A.; Enomoto, H.; Kishida, H.; Moriya, T. A new hydrothermal process for producing acetic acid from biomass waste. *Chem. Eng. Res. Des.* **2007** 201–206. https://doi.org/10.1205/cherd06020.

[11] Kumar, A.; Sinha, A.S.K. Comparative study of hydrogen production from steam reforming of acetic acid over synthesized catalysts via MOF and wet impregnation methods. *Int. J. Hydrogen Energy.* **2020** 11512–11526. https://doi.org/10.1016/j.ijhydene.2020.02.097.

[12] Hu, X.; Yang, J.; Sun, W.; Wang, N.; An, S.; Wang, Q.; Zhang, Y.; Xie, X.; Huang, L. Y-Zr-O solid solution supported Ni-based catalysts for hydrogen production via auto-thermal reforming of acetic acid. *Appl. Catal. B Environ.* **2020** 119264. https://doi.org/10.1016/j.apcatb.2020.119264.

[13] Cakiryilmaz, N.; Arbag, H.; Oktar, N.; Dogu, G.; Dogu, T. Catalytic performances of Ni and Cu impregnated MCM-41 and Zr-MCM-41 for hydrogen production through steam reforming of acetic acid. *Catal. Today.* **2019** 191–199. https://doi.org/10.1016/j.cattod.2018.06.004.

[14] Chen, G.; Tao, J.; Liu, C.; Yan, B.; Li, W.; Li, X. Hydrogen production via acetic acid steam reforming: A critical review on catalysts. *Renew. Sustain. Energy Rev.* **2017** 1091–1098. https://doi.org/10.1016/j.rser.2017.05.107.

[15] Zhou,Q.; Zhong, X.; Xie, X.; Jia, X.; Chen, B.; Wang, N.; Huang, L. Auto-thermal reforming of acetic acid for hydrogen production by ordered mesoporous Ni-xSm-Al-O catalysts: Effect of samarium promotion. *Renew. Energy.* **2020** 2316–2326. https://doi.org/10.1016/j.renene.2019.07.078.

[16] Choi, I.H; Hwang, K.R.; Lee, K.Y.; Lee, I.G. Catalytic steam reforming of biomass-derived acetic acid over modified Ni/Γ-Al_2O_3 for sustainable hydrogen production. *Int. J. Hydrogen Energy.* **2019** 180–190. https://doi.org/10.1016/j.ijhydene.2018.04.192.

[17] Navarro, R.M.; Guil-Lopez, R.; Ismail, A.A.; Al-Sayari, S.A.; Fierro, J.L.G. Ni- and PtNi-catalysts supported on Al_2O_3 for acetone steam reforming: Effect of the modification of support with Ce, La and Mg. *Catal. Today.* **2015** 60–70. https://doi.org/10.1016/j.cattod.2014.07.036.

[18] Matas Güell, B.; Babich, I.; Nichols, K.P.; Gardeniers, J.G.E.; Lefferts, L.; Seshan, K. Design of a stable steam reforming catalyst-A promising route to sustainable hydrogen from biomass oxygenates. *Appl. Catal. B Environ.* **2009** 38–44. https://doi.org/10.1016/j.apcatb.2009.02.008.

[19] Pu, J.; Nishikado, K.; Wang, N.; Nguyen, T.T.; Maki, T.; Qian, E.W. Core-shell nickel catalysts for the steam reforming of acetic acid. *Appl. Catal. B Environ.* **2018** 69–79. https://doi.org/10.1016/j.apcatb.2017.09.058.

[20] Resende, K.A.; Ávila-Neto, C.N.; Rabelo-Neto, R.C.; Noronha, F.B.; Hori, C.E. Hydrogen production by reforming of acetic acid using La-Ni type perovskites partially substituted with Sm and Pr. *Catal. Today.* **2015** 71–79. https://doi.org/10.1016/j.cattod.2014.07.013.

[21] Pu, J.; Luo, Y.; Wang, N.; Bao, H.; Wang, X.; Qian, E.W. Ceria-promoted Ni@Al_2O_3 core-shell catalyst for steam reforming of acetic acid with enhanced activity and coke resistance. *Int. J. Hydrogen Energy.* **2018** 3142–3153. https://doi.org/10.1016/j.ijhydene.2017.12.136.

[22] Batista da Silva, R.; Brandão, S.T.; Lucotti, A.; Tommasini, M.S.; Castiglioni, C.; Groppi, G.; Beretta, A. Chemical pathways in the partial oxidation and steam reforming of acetic acid over a Rh-Al_2O_3 catalyst. *Catal. Today.* **2017** 162–172. https://doi.org/10.1016/j.cattod.2016.08.018.

Preprints (www.preprints.org) | NOT PEER-REVIEWED | Posted: 23 December 2020 doi:10.20944/preprints202012.0573.v1

[23] Veiga, S.; Romero, M.; Faccio, R.; Segobia, D.; Duarte, H.; Apesteguía, C.; Bussi, J. Hydrogen-rich gas production by steam and oxidative steam reforming of crude glycerol over Ni-La-Me mixed oxide catalysts (Me= Ce and/or Zr). *Catal. Today.* 2019. https://doi.org/10.1016/j.cattod.2019.02.008.
[24] Takanabe, K.; Aika, K.; Seshan, K.; Lefferts, L. Catalyst deactivation during steam reforming of acetic acid over Pt/ZrO_2. *Chem. Eng. J.* **2006** 133–137. https://doi.org/10.1016/j.cej.2006.04.001.
[25] Pant, K.K.; Mohanty, P.; Agarwal, S.; Dalai, A.K. Steam reforming of acetic acid for hydrogen production over bifunctional Ni-Co catalysts. *Catal. Today.* **2013** 36–43. https://doi.org/10.1016/j.cattod.2012.06.021.
[26] Hu, X.; Dong, D.; Shao, X.; Zhang, L.; Lu, G. Steam reforming of acetic acid over cobalt catalysts: Effects of Zr, Mg and K addition. *Int. J. Hydrogen Energy.* **2017** 4793–4803. https://doi.org/10.1016/j.ijhydene.2016.12.033.
[27] Zhang, F.; Wang, N.; Yang, L.; Li, M.; Huang, L. Ni-Co bimetallic MgO-based catalysts for hydrogen production via steam reforming of acetic acid from bio-oil. *Int. J. Hydrogen Energy.* **2014** 18688–18694. https://doi.org/10.1016/j.ijhydene.2014.01.025.
[28] Hu, X.; Lu, G. The inhibition effect of potassium addition on methane formation in steam reforming of acetic acid over alumina-supported cobalt catalysts. *Chem. Lett.* **2008** 614–615. https://doi.org/10.1246/cl.2008.614.
[29] Basagiannis, A.C.; Verykios, X.E.; Catalytic steam reforming of acetic acid for hydrogen production. *Int. J. Hydrogen Energy.* **2007** 3343–3355. https://doi.org/10.1016/j.ijhydene.2007.04.039.
[30] Megía, P.J.; Carrero, A.; Calles, J.A.; Vizcaíno, A.J. Hydrogen production from steam reforming of acetic acid as a model compound of the aqueous fraction of microalgae HTL using Co-M/SBA-15 (M: Cu, Ag, Ce, Cr) catalysts. *Catalysts.* **2019** 1013. https://doi.org/10.3390/catal9121013.
[31] Zhao, D.; Feng, J.; Huo, Q.; Melosh, N.; Fredrickson, G.H.; Chmelka, B.F.; Stucky, G.D. Triblock copolymer syntheses of mesoporous silica with periodic 50 to 300 angstrom pores. *Science* **1998** 548–552. https://doi.org/10.1126/science.279.5350.548.
[32] Singh, S.; Kumar, R.; Setiabudi, H.D.; Nanda, S.; Vo, D.V.N. Advanced synthesis strategies of mesoporous SBA-15 supported catalysts for catalytic reforming applications: A state-of-the-art review. *Appl. Catal. A Gen.* **2018** 57–74. https://doi.org/10.1016/j.apcata.2018.04.015.
[33] Chaudhary, V.; Sharma, S. An overview of ordered mesoporous material SBA-15 : synthesis , functionalization and application in oxidation reactions Microporous Mesoporous Macroporous. *J. Porous Mater.* **2017** 741–749. https://doi.org/10.1007/s10934-016-0311-z.
[34] Garcia, L.; French, R.; Czernik, S.; Chornet, E. Catalytic steam reforming of bio-oils for the production of hydrogen: Effects of catalyst composition. *Appl. Catal. A Gen.* **2000** 225–239. https://doi.org/10.1016/S0926-860X(00)00440-3.
[35] Yaseneva, P.; Pavlova, S.; Sadykov, V.; Moroz, E.; Burgina, E.; Dovlitova, L.; Rogov, V.; Badmaev, S.; Belochapkin, S.; Ross, J. Hydrogen production by steam reforming of methanol over Cu-CeZrYOx-based catalysts. *Catal. Today.* **2008** 175–182. https://doi.org/10.1016/j.cattod.2008.06.012.
[36] Calles, J.A.; Carrero, A.; Vizcaíno, A.J.; Megía, P.J. Agglomerated Co-Cr/SBA-15 catalysts for hydrogen production through acetic acid steam reforming. *Int. J. Hydrogen Energy*. **2019** 1–10. https://doi.org/10.1016/j.ijhydene.2019.05.237.
[37] Pu, J.; Ikegami, F.; Nishikado, K.; Qian, E.W. Effect of ceria addition on Ni-Ru/CeO_2-Al_2O_3 catalysts in steam reforming of acetic acid. *Int. J. Hydrogen Energy.* **2017** 19733–19743. https://doi.org/10.1016/j.ijhydene.2017.06.120.
[38] Lemonidou, A.A.; Vagia, E.C.; Lercher, J.A. Acetic acid reforming over Rh supported on La_2O_3/CeO_2-ZrO_2: Catalytic performance and reaction pathway analysis. *ACS Catal.* **2013** 1919–1928. https://doi.org/10.1021/cs4003063.
[39] Palma, V.; Ruocco, C.; Meloni, E.; Gallucci, F.; Ricca, A. Enhancing Pt-Ni/CeO_2 performances for ethanol reforming by catalyst supporting on high surface silica. *Catal. Today.* **2018** 175–188. https://doi.org/10.1016/j.cattod.2017.05.034.
[40] Cai, W.; Wang, F.; Van Veen, A.C.; Provendier, H.; Mirodatos, C.; Shen, W. Autothermal reforming of ethanol for hydrogen production over an Rh/CeO_2 catalyst. *Catal. Today.* **2008** 152–156. https://doi.org/10.1016/j.cattod.2008.05.019.
[41] Iulianelli, A.; Liguori, S.; Vita, A.; Italiano, C.; Fabiano, C.; Huang, Y.; Basile, A. The oncoming energy vector: Hydrogen produced in Pd-composite membrane reactor via bioethanol reforming over Ni/CeO_2 catalyst. *Catal. Today.* **2016** 368–375. https://doi.org/10.1016/j.cattod.2015.04.046.
[42] Araiza, D.G.; Gómez-Cortés, A.; Díaz, G. Effect of ceria morphology on the carbon deposition during steam reforming of ethanol over Ni/CeO_2 catalysts. *Catal. Today.* **2020** 235–243. https://doi.org/10.1016/j.cattod.2018.03.016.
[43] Sutthisripok, W.; Sattayanurak, S.; Sikong, L. Effect of specific surface area on oxygen storage capacity (OSC) and methane steam reforming reactivity of CeO_2. *J. Porous Mater.* **2008** 519–525. https://doi.org/10.1007/s10934-007-9107-5.
[44] Palma, V.; Ruocco, C.; Meloni, E.; Ricca, A. Oxidative steam reforming of ethanol on mesoporous silica supported Pt–Ni/CeO_2 catalysts. *Int. J. Hydrogen Energy*. **2017** 1598–1608. https://doi.org/10.1016/j.ijhydene.2016.05.071.
[45] Martínez, A.; López, C.; Márquez, F.; Díaz, I. Fischer – Tropsch synthesis of hydrocarbons over mesoporous Co/SBA-15 catalysts: the influence of metal loading, cobalt precursor, and promoters. *J. Catal* **2003** 486–499. https://doi.org/10.1016/S0021-9517(03)00289-6.
[46] Grzybowska, B.; Słoczyński, J.; Grabowski, R.; Wcisło, K.; Kozłowska, A.; Stoch, J.; Zieliński, J. Chromium oxide/alumina catalysts in oxidative dehydrogenation of isobutane. *J. Catal.* **1998** 687–700. https://doi.org/10.1006/jcat.1998.2203.
[47] Yao, H.C.; Yao, Y.F.Y. Ceria in automotive exhaust catalysts. *J. Catal.* **1984** 254–265. https://doi.org/10.1016/0021-9517(84)90371-3.
[48] De Lima, S.M.; Adriana, M.; Lídia, O.O.; Graham, U.M.; Jacobs, G.; Davis, B.H.; Mattos, L.; Noronha, F.B. Study of catalyst deactivation and reaction mechanism of steam reforming , partial oxidation , and oxidative steam reforming of ethanol over Co/CeO_2 catalyst. *J. Catal.* **2009** 268–281. https://doi.org/10.1016/j.jcat.2009.09.025.

Preprints (www.preprints.org) | NOT PEER-REVIEWED | Posted: 23 December 2020 doi:10.20944/preprints202012.0573.v1

[49] Wang, L.; Liu, H;. Chen, Y.; Zhang, R.; Yang, S. K-Promoted Co-CeO_2 catalyst for the reverse watergas shift reaction. *Chem. Lett.* **2013** 682–683. https://doi.org/10.1246/cl.130137.
[50] Costa, A.F.; Cerqueira, H.S.; Falabella, E.; Aguiar, S.; Rollán, J.; Martínez, A. New supports for co-based fischer-tropsch catalyst. *Stud. Surf. Sci. Catal.* **2007** 141–146. https://doi.org/10.1016/S0167-2991(07)80122-4.
[51] El Hassan, N.; Kaydouh, M.N.; Geagea, H.; El Zein, H.; Jabbour, K.; Casale, S.; El Zakhem, H.; Massiani, P. Low temperature dry reforming of methane on rhodium and cobalt based catalysts: Active phase stabilization by confinement in mesoporous SBA-15. *Appl. Catal. A Gen.* **2016** 114–121. https://doi.org/10.1016/j.apcata.2016.04.014.
[52] Chen, J.; Zhang, X.; Arandiyan, H.; Peng, Y.; Chang, H.; Li, J. Low temperature complete combustion of methane over cobalt chromium oxides catalysts, *Catal. Today.* **2013** 12–18. https://doi.org/10.1016/j.cattod.2012.03.026
[53] Greluk, M.; Rotko, M.; Turczyniak-Surdacka, S. Enhanced catalytic performance of La_2O_3 promoted Co/CeO_2 and Ni/CeO_2 catalysts for effective hydrogen production by ethanol steam reforming: La_2O_3 promoted Co(Ni)/CeO_2 catalysts in SRE. *Renew. Energy.* **2020** 378–395. https://doi.org/10.1016/j.renene.2020.03.117.
[54] Wu, X.; Liu, S;. Weng, D.; Lin, F.; Ran, R. MnO_x-CeO_2-Al_2O_3 mixed oxides for soot oxidation: Activity and thermal stability. *J. Hazard. Mater.* **2011** 283–290. https://doi.org/10.1016/j.jhazmat.2011.01.010.
[55] Carrero, A.; Calles, J.A.; García-Moreno, L.; Vizcaíno, A.J. Production of renewable hydrogen from glycerol steam reforming over bimetallic Ni-(Cu,Co,Cr) catalysts supported on SBA-15 silica. *Catalysts.* **2017** 55. https://doi.org/10.3390/catal7020055.
[56] Calaza, F.C.; Chen, T.L.; Mullins, D.R.; Xu, Y.; Overbury, S.H. Reactivity and reaction intermediates for acetic acid adsorbed on CeO_2(1 1 1). *Catal. Today.* **2015** 65–76. https://doi.org/10.1016/j.cattod.2015.03.033.
[57] Snell, R.W.; Shanks, B.H.; Insights into the ceria-catalyzed ketonization reaction for biofuels applications. *ACS Catal.* **2013** 783–789. https://doi.org/10.1021/cs400003n.
[58] Wu, Z.; Mann, A.K.P.; Li, M.; Overbury, S.H. Spectroscopic investigation of surface dependent acid base property of ceria nanoshapes. *J. Phys. Chem. C.* **2015** 7340–7350. https://doi.org/10.1021/acs.jpcc.5b00859.
[59] Baylon, R.A.L.; Sun, J.; Martin, K.J.; Venkitasubramanian, P.; Wang, Y. Beyond ketonization: Selective conversion of carboxylic acids to olefins over balanced Lewis acid-base pairs. *Chem. Commun.* **2016** 4975–4978. https://doi.org/10.1039/c5cc10528e.
[60] Qian, L.; Cai, W.; Zhang, L.; Ye, L.; Li, J.; Tang, M.; Yue, B.; He, H. The promotion effect of hydrogen spillover on CH_4 reforming with CO_2 over Rh/MCF catalysts. *Appl. Catal. B Environ.* **2015** 168–175. https://doi.org/10.1016/j.apcatb.2014.09.006.